PCCP

PAPER

View Article Online
View Journal | View Issue

Cite this: *Phys. Chem. Chem. Phys.*, 2019, **21**, 15798

Single-layer structures of a_{100}- and b_{010}-Gallenene: a tight-binding approach†

M. Nakhaee,[ab] M. Yagmurcukardes,* [a] S. A. Ketabi[b] and F. M. Peeters[a]

Received 3rd May 2019,
Accepted 20th June 2019

DOI: 10.1039/c9cp02515d

rsc.li/pccp

Using the simplified linear combination of atomic orbitals (LCAO) method in combination with *ab initio* calculations, we construct a tight-binding (TB) model for two different crystal structures of monolayer gallium: a_{100}- and b_{010}-Gallenene. The analytical expression for the Hamiltonian and numerical results for the overlap matrix elements between different orbitals of the Ga atoms and for the Slater and Koster (SK) integrals are obtained. We find that the compaction of different structures affects significantly the formation of the orbitals. The results for a_{100}-Gallenene can be very well explained with an orthogonal basis set, while for b_{010}-Gallenene we have to assume a non-orthogonal basis set in order to construct the TB model. Moreover, the transmission properties of nanoribbons of both monolayers oriented along the AC and ZZ directions are also investigated and it is shown that both AC- and ZZ–b_{010}-Gallenene nanoribbons exhibit semiconducting behavior with zero transmission while those of a_{100}-Gallenene nanoribbons are metallic.

1 Introduction

Following the successful synthesis of graphene[1,2] from its bulk crystal, graphite, two-dimensional (2D) materials have gained a lot of interest in nanodevice applications owing to their extraordinary properties.[3–6] In recent years, researchers have paid special attention to the synthesis of monolayers of other mono-atomic crystals such as silicene[7–9] germanene,[10–13] stanene,[14,15] phosphorene[16] and borophene[17] due to their specific electronic properties.[18–22]

A wide range of 2D materials ranging from graphene to topological insulators[23–28] share the extraordinary phenomenon that electrons behave as relativistic particles in their low-energy excitations. This emergent behavior of fermions in condensed matter systems has been classified as ''Dirac materials'' which have attracted both experimental and theoretical interest. Recently, fully metallic gallium-based 2D crystals, named as 'Gallenene' have been synthesized on different substrates.[29,52]

Gallium is a metallic element and it is known to exhibit metallicity in its bulk crystal.[30] It was also reported to be a non-toxic liquid metal at room temperature.[31,32] In its bulk form, gallium exhibits various types of phases such as boron-like molecular and close-packed metallic which are known to exist under non-standard pressure and temperature.[31,33,34] Moreover, the extreme covalent bonding character of the Ga_2 pairs causes the pairs to exhibit dimer-like behavior. The α-Ga, a phase of bulk-gallium, is known as the only one which reveals both metallic and molecular character at zero pressure.[31]

We construct a tight-binding (TB) model[35,36] whose parameters are determined through a nonlinear fitting algorithm of the energy bands that are obtained by *ab initio* methods. The TB model can provide us the hoppings and overlaps between different orbitals of the atoms. The Slater and Koster scheme (SK)[37] and the Naval Research Laboratory (NRL) method,[38] as an extension of the SK approach, are two powerful methods for reproducing the first-principles data in terms of a set of non-interacting single-particles. The SK method gives the hopping between the orbitals for each bond separately while NRL also gives the hoppings as a function of distance up to a certain cut-off radius. In 1954, J. C. Slater and G. F. Koster[38] represented the expectation values of the matrix elements of the Hamiltonian in the basis of the directed orbitals in terms of eight integrals ($v_{ss\sigma}$, $v_{sp\sigma}$, $v_{pp\sigma}$, $v_{pp\pi}$, $s_{ss\sigma}$, $s_{sp\sigma}$, $s_{pp\sigma}$, $s_{pp\pi}$).

The understanding of electronic transport of materials is one of the interesting fields of research among the 2D systems. A significant exploratory research study into 2D materials has been done using Green's function theory for which we need the TB model. Here, we apply the SK method and present the coefficients for different bonds.

The Slater–Koster integrals for different Ga–Ga bonds are found up to the second nearest neighbors. The b_{010}-Gallenene structure is more compact than the a_{100}-Gallenene and

[a] *Department of Physics, University of Antwerp, Groenenborgerlaan 171, B-2020 Antwerp, Belgium. E-mail: mohammad.nakhaee@uantwerpen.be, mehmetyagmurcukardes.edu@gmail.com, francois.peeters@uantwerpen.be*

[b] *School of Physics, Damghan University, P.O. Box 36716-41167, Damghan, Iran. E-mail: saketabi@du.ac.ir*

† Electronic supplementary information (ESI) available: See the supplementary materials for the complete set of SK matrix elements. See DOI: 10.1039/c9cp02515d

consequently, the orbitals are substantially different from the pure atomic-like shape. Compaction of the structures can affect significantly the overlap between orbitals and result in a non-unitary overlap matrix. a_{100}-Gallenene exhibits a graphene-like planar structure and can be modelled by an orthogonal basis while for the b_{010}-Gallenene a non-orthogonal basis set is needed.

2 Computational methodology

For structural optimization and electronic-band structure calculations of the monolayers of a_{010}- and b_{100}-Gallenene crystals, first principles calculations were performed in the framework of density functional theory (DFT) as implemented in the Vienna *ab initio* simulation package (VASP).[39] The Perdew–Burke–Ernzerhof (PBE)[40] form of the generalized gradient approximation (GGA) was adopted to describe electron exchange and correlation. The electronic-band structures were calculated at the GGA level.

The kinetic energy cut-off for plane-wave expansion was set to 500 eV and the energy was minimized until its variation in subsequent steps became 10^{-8} eV. The Gaussian smearing method was employed for the total energy calculations and the width of the smearing was chosen as 0.05 eV. Total Hellmann–Feynman forces in the primitive unit cell were reduced to 10^{-7} eV Å^{-1} for structural optimization. $19 \times 19 \times 1$ Γ centered k-point samplings were used in the primitive unit cells. To avoid interaction between the neighboring layers, our calculations were implemented with a vacuum space of 15 Å.

3 Structural and electronic properties

In this section, the structural and electronic properties of mono-atomic monolayers of gallium, a_{100}- and b_{010}-Gallenene, are discussed in detail. The optimized unit cell of each crystal structure has four Ga atoms as shown in Fig. 1(a) and (b). As mentioned by Kockat *et al.*,[29] the relaxed crystal structures of both monolayers exhibit imaginary frequencies through the whole Brillouin Zone (BZ) which reveals the dynamical instability in their free-standing forms. However, it was also demonstrated that both of the monolayer crystals can be stabilized upon application of a biaxial strain (6% and 2% for a_{100}- and b_{010}-Gallenene, respectively). Therefore, in this work we consider biaxially straining, *i.e.* we investigate the dynamically stable structures, which can be realized by using an appropriate substrate.

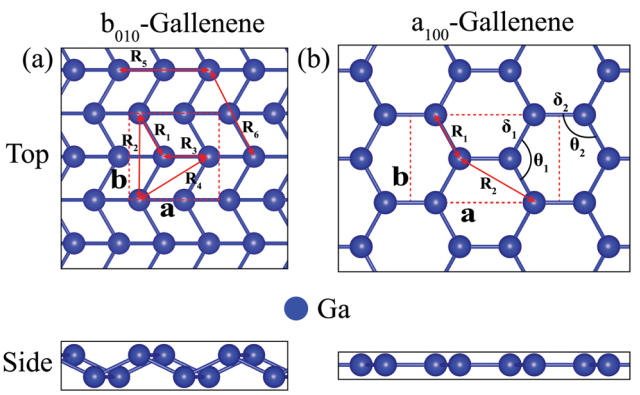

Fig. 1 The optimized structure of (a) a_{100}-Gallenene and (b) b_{010}-Gallenene. The unit cell is given by the dotted box. R_i denotes the distance between the Ga atoms.

The monolayer of a_{100}-Gallenene has a honeycomb structure with a rectangular primitive unit cell. The lattice constants a and b are found to be 7.87 and 4.65 Å, respectively. The Ga–Ga bond lengths are nearly equal because the two nearest neighbors of a Ga atom are both at 2.66 Å (δ_1) and the third one is at 2.67 Å (δ_2). These bond lengths are larger than those between other group-IV atoms in a group-IV mono-atomic monolayer that is attributed to the larger atomic radius of Ga. Moreover, different interior angles (122.43° and 118.80° for θ_1 and θ_2, respectively) in a_{100}-Gallenene suggest that the hybridization in the crystal structure is not completely sp^2 despite the planar structure. Different from the 2-atom primitive hexagonal unit cell of graphene which belongs to the space group symmetry of $P\bar{6}/mmm$, the primitive unit cell of a_{100}-Gallenene is slightly distorted which belongs to the *Pbam* space group symmetry. In addition, the point symmetry of a_{100}-Gallenene turns into D_{2h} which is known to be D_{6h} for graphene.

The monolayer b_{010}-Gallenene resembles a zigzag rhombic lattice which exhibits lower symmetry than a_{100}-Gallenene. The lattice constants a and b, in this case, are calculated to be 4.74 and 4.92 Å, respectively. The Ga–Ga bond length is 2.73 Å which is larger than that of a_{100}-Gallenene due to the buckled structure of b_{010}-Gallenene. In the quasi-2D multi-decker structure, the vertical direction between Ga-dimers, or the buckling height, is calculated to be 1.19 Å. Such buckling can also be seen in other monoatomic monolayer crystals such as silicene, germanene, stanene, and black phosphorus.

In order to analyze the electronic properties of monolayers of a_{100}- and b_{010}-Gallenene, the orbital-projected electronic-band structures are calculated within the DFT-based methods (see Fig. 2). It is clear that both the monolayer crystals exhibit metallic character because of the finite number of bands crossing the Fermi level. As shown in Fig. 2, the unoccupied p_z orbitals in planar a_{100}-Gallenene creates Dirac cones which lie above the Fermi level. In the case of b_{010}-Gallenene, the p_z orbitals are hybridized with the in-plane orbitals due to the buckled crystal structure. Therefore, the bands are highly dispersive in monolayer b_{010}-Gallenene.

4 Tight-binding model

In DFT, we have in principle an infinite number of atoms with an infinite number of orbitals to explain the electronic structure of the different crystal structures. With the linear combination of atomic orbitals (LCAO), we are able to limit the system up to a finite number of atoms and a finite number of orbitals per atom and thus, the Bloch theorem can be effectively applied through a TB model. We use these orbitals as the basis set to represent the

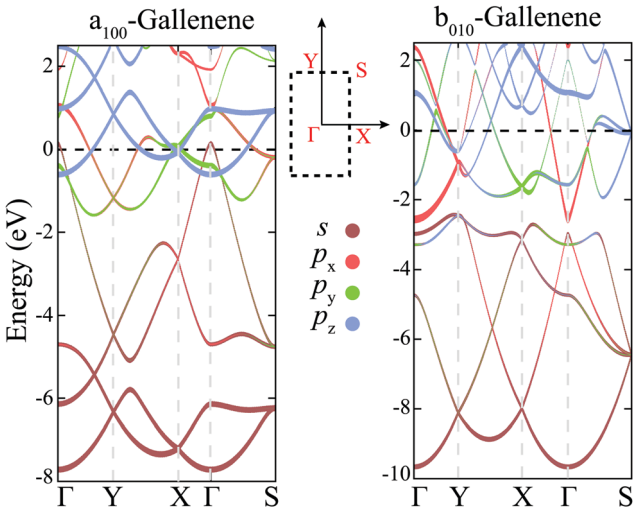

Fig. 2 The electronic-band structure of a_{100}-Gallenene (left side) and b_{010}-Gallenene (right side). The different colors of the bands refer to the different orbital contribution. The dashed rectangle indicates the BZ with the high symmetry points.

wave function. The Bloch function with a well-defined k vector can be generally expanded as linear combinations of the orbitals φ as follows

$$\psi_k(\mathbf{r}) = \sum_{\nu'} \sum_{i'} c_{i'\nu'}(k)\phi_{\nu,k}(\mathbf{r} - \mathbf{r}_i) \quad (1)$$

in which i and ν run over the atoms in the unit cell and the orbitals s, p_x, p_y and p_z, respectively. In the case of a_{100}-Gallenene and b_{010}-Gallenene we have four orbitals per atom and so 16 orbitals per unit cell. $\phi_{\nu,\mathbf{k}}(\mathbf{r})$ is defined as follows

$$\phi_{\nu,\mathbf{k}}(\mathbf{r}) = \sum_{n\in\mathbb{Z}} \sum_{m\in\mathbb{Z}} e^{i\mathbf{k}.\mathbf{R}_{n,m}} \varphi_\nu(\mathbf{r} - \mathbf{R}_{n,m}) \quad (2)$$

where $\mathbf{R}_{n,m}$ is the discrete translation vector of the unit cell at (m,n). We limit the interactions up to the first nearest unit cell. We follow the SK scheme in combination with the usual Levenberg–Marquardt nonlinear fitting algorithm[41] to find the best hoppings for both Hamiltonian and overlap matrices.

For both structures, we have a basis of four Ga atoms and we assume a basis of four orbitals (s, p_x, p_y and p_z) per atom, which generates a band structure with 8 valence and 8 conduction bands. So, we have in total 16 bands and we focus on the first 11 bands in the case of a_{100}-Gallenene and the first 10 bands for b_{010}-Gallenene. The generalized eigenvalue equation for the TB model may be written as follows;[42]

$$\sum_{\nu'} \sum_{i'} [H_{i\nu,i'\nu'} - \varepsilon_k S_{i\nu,i'\nu'}] c_{i'\nu'}(k) = 0, \quad (3)$$

in which H is the mono-electronic Hamiltonian and S is the overlap matrix which is dimensionless. The basis can be formed not orthonormal,[43–45] but in the case of an orthogonal basis set (a_{100}-Gallenene) the overlap matrix is a unity matrix and can be ignored from the expression. The expectation values for the Hamiltonian and overlap matrix can be written in terms of distances in real space as follows

$$H_{i\nu,i'\nu'} = \langle \phi_\nu(r - r_i)|H|\phi_{\nu'}(r - r_{i'})\rangle,$$
$$S_{i\nu,i'\nu'} = \langle \phi_\nu(r - r_i)|\phi_{\nu'}(r - r_{i'})\rangle. \quad (4)$$

The integrals are calculated over the whole unit cell and i and ν run over the atoms in the unit cell and the orbitals s, p_x, p_y and p_z, respectively. Theoretically, the inter-atomic matrix elements in eqn (4) can in principle be calculated directly from the known wave functions, but alternatively, we can use the fitting algorithm to find the best values for the integrals. The expectation values may be written in terms of the directional cosines ($n_i = \mathbf{r}\cdot\mathbf{e}_i/|\mathbf{r}|$) as follows;

$$\langle s|H|s\rangle = v_{ss\sigma},$$

$$\langle s|H|p_i\rangle = n_i v_{sp\sigma},$$

$$\langle p_i|H|p_j\rangle = (\delta_{ij} - n_i n_j)v_{pp\pi} + n_i n_j v_{pp\sigma},$$

where $\mathbf{r}$ is the vector along the bond while i is x, y and z. The corresponding expressions for the overlap matrix can be found by replacing H by S and v by s. Note that one should consider the rule of angular quantum number $(\langle l|H|l'\rangle = (-1)^{l+l'}\langle l'|H|l\rangle)$ to evaluate complex conjugated hopping matrix elements.

To calculate the TB Hamiltonian by using the eight Slater–Koster integrals, one needs to know the inter-atomic distances. In Fig. 1 the distance between two Ga atoms is shown by R_i where i refers to different types of bonds. After optimizing the atomic positions, we find the distances R_1 = 2.655 Å, R_2 = 2.656 Å, R_3 = 4.572 Å and R_4 = 4.654 Å for a_{100}-Gallenene and R_1 = 2.732 Å, R_2 = 4.744 Å, R_3 = 2.876 Å and R_4 = 4.649 Å for b_{010}-Gallenene.

The complicated electronic dispersion bands and the compact structure of b_{010}-Gallenene exhibit a sp^3 hybridization. By making a comparison between the atomic packing factor (APF)[46] of a_{100}-Gallenene and b_{010}-Gallenene one can find $APF_{b_{010}} = 1.71APF_{a_{100}}$, which is the reason why we choose a non-orthogonal basis set for the structure of b_{010}-Gallenene. For both the structures we have found the Slater–Koster integrals of the Ga–Ga bonds up to the second nearest neighbors which result in a satisfactory fitting of the band structure (see Fig. 3). In Table 1, we list the Slater–Koster parameters of both systems in terms of bond length and bond type as obtained by fitting the DFT energy bands shown in Fig. 3. The on-site parameters of the Ga atoms are presented in Table 2. The TB model for b_{010}-Gallenene can be also defined orthogonally but with taking more neighbors into account.

In the case of a_{100}-Gallenene the distance between the atoms is large enough to assume that the orbitals are orthogonal, but to construct a TB model for b_{010}-Gallenene, since the structure is compact we need to assume a non-orthogonal set of orbitals or alternatively we can construct an orthogonal TB model with taking more bonds into account. In the orthogonal model of

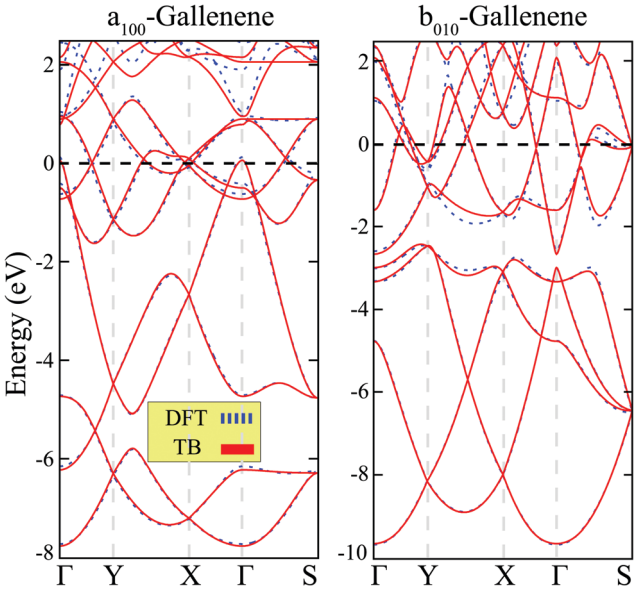

Fig. 3 The band structure of a_{100}-Gallenene (left side) and b_{010}-Gallenene (right side) calculated within DFT (dashed blue lines) and from the TB model (solid red lines).

Table 1 The Slater–Koster parameters for a_{100}-Gallenene (top) and b_{010}-Gallenene (bottom). The V parameters are in eV, and the S parameters are dimensionless

R	$V_{ss\sigma}$	$V_{sp\sigma}$	$V_{pp\sigma}$	$V_{pp\pi}$	$S_{ss\sigma}$	$S_{sp\sigma}$	$S_{pp\sigma}$	$S_{pp\pi}$
R_1	−1.304	−1.605	2.313	−0.579	0	0	0	0
R_2	0.016	0.034	0.227	−0.058	0	0	0	0

R	$V_{ss\sigma}$	$V_{sp\sigma}$	$V_{pp\sigma}$	$V_{pp\pi}$	$S_{ss\sigma}$	$S_{sp\sigma}$	$S_{pp\sigma}$	$S_{pp\pi}$
R_1	−1.003	−2.167	1.944	−0.662	0.030	0.205	−0.334	0.270
R_2	−0.147	−0.113	0.608	−0.030	0.027	0.015	−0.071	0.055
R_3	−1.176	−2.353	1.300	−0.795	0.017	0.141	−0.367	0.082
R_4	0.303	−0.146	0.636	−0.063	−0.034	−0.003	−0.035	−0.025

Table 2 The on-site energies for a_{100}-Gallenene and b_{010}-Gallenene in units of eV

	a_{100}-Gallenene				b_{010}-Gallenene			
	s	p_x	p_y	p_z	s	p_x	p_y	p_z
Ga	−3.934	2.969	2.992	1.377	−4.378	−0.099	0.601	0.682

b_{010}-Gallenene we used R_1, R_2, R_3 and R_4 while for the orthogonal model we should add more bonds.

To explain the system orthogonally we add the hopping between the orbitals of the Ga atoms with the distance R_5 and R_6 (see Fig. 1). The SK parameters and on-sites of the orthogonal TB model of b_{010}-Gallenene are presented in Tables 3 and 4.

The bandstructure of the orthogonal TB model of b_{010}-Gallenene is presented in Fig. 4. It can be seen that taking more neighbors into account is equivalent to a defined non-orthogonal basis set for orbitals that both cases can result in more real interactions between the Ga atoms.

Table 3 Orthogonal Slater–Koster parameters for b_{010}-Gallenene in eV

R	$V_{ss\sigma}$	$V_{sp\sigma}$	$V_{pp\sigma}$	$V_{pp\pi}$
R_1	−0.612	−1.855	0.966	−0.634
R_2	−0.176	0.042	−0.163	0.126
R_3	−0.771	−1.433	1.148	−0.831
R_4	0.013	0.073	−0.431	0.126
R_5	−0.025	0.098	−0.100	0.108
R_6	−0.249	−0.175	0.156	0.019

Table 4 The on-site energies of the orthogonal TB model of b_{010}-Gallenene in units of eV

	b_{010}-Gallenene			
	s	p_x	p_y	p_z
Ga	−3.188	1.052	1.907	1.393

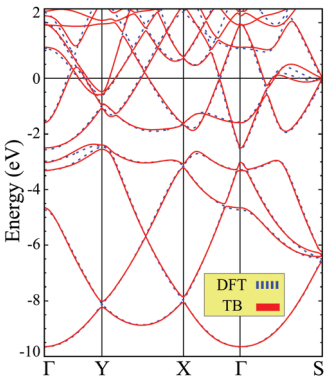

Fig. 4 The electronic-band structure of b_{010}-Gallenene using orthogonal SK parameters.

Using the Slater–Koster parameters one can calculate the coupling matrices between different unit cells in terms of hoppings between different orbitals (see ESI† [47]).

5 Transmission and density of states

Electronic transport is one of the most interesting properties of 2D materials. Here our methodology is based on the Green's function approach in the tight-binding approximation. For a 2D system, transmission and density of states (DOS) have been calculated in x (armchair, AC,) and y (zigzag, ZZ,) directions. The Green's function method is a powerful method to study the electronic properties in which the most important property of the physical observables in transport, such as electrical current, is the transmission. The tight-binding description of transmission through a junction has been interesting for scientists to observe how much an electron wave packet would transmit in a specific energy. One needs the Hamiltonian of the system which is expressed in the tight-binding approximation. The routine method based upon a formulation for the conductance in terms of Green's functions, G, is the well known Fisher–Lee linear-response[48] for the conductance of a

finite lattice embedded between the leads. We represent our results for AC and ZZ nanoribbons of a_{100}-Gallenene and b_{010}-Gallenene structures. At this point, it is necessary to discuss that for a nanoribbon, the transmission $T(\varepsilon)$ can be calculated as follows:

$$T(\varepsilon) = \mathrm{Re}\left(\mathrm{Tr}\left(\sum_{l} G \cdot \sum_{r} G^{\dagger}\right)\right) \quad (5)$$

To have complete information about a solid, all possible states should be taken into account. The number of occupied available states as a function of energy is important for the calculations of the band theory like transition probability,[49] conductivity calculation and computing scattering rates.[50,51] The Green's function of the Hamiltonian of the system is a key concept with important links for the concept of density of state as follows;

$$\mathrm{DOS}(\varepsilon) = \frac{-1}{\pi}\mathrm{Im}(\mathrm{Tr}(G)) \quad (6)$$

Fig. 5 shows the nanoribbon made of a_{100}-Gallenene and b_{010}-Gallenene unit-cells in both x and y directions. The width of the nanoribbon can be determined by the parameter N which determines the number of repetitions of the unit-cell in the non-periodic direction. The green part indicates the unit-cell of the 2D nanosheet. By growing the 2D unit-cell one can construct any finite or infinite structure and calculate the band energies of different nanoribbons with different widths (see ESI† [47]).

Using the SK parameters mentioned in Section 4, the TB Hamiltonian can be constructed (see ESI†[47]). Note that the Hamiltonian matrix for a nanoribbon can be generated from the blocks of a 2D Hamiltonian matrix. Fig. 6 shows the band structure of the nanoribbons of both monolayers with N = 2. It is found that a_{100}-Gallenene nanoribbons exhibit metallic behavior for orientations while b_{010}-Gallenene nanoribbons display semiconducting behavior.

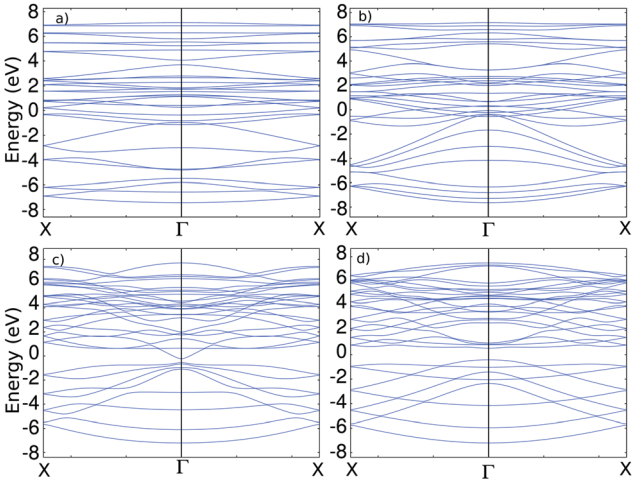

Fig. 6 The electronic-band structure of the nanoribbons of a_{100}-Gallenene in AC (a) and ZZ (b) directions and b_{010}-Gallenene in AC (c) and ZZ (d) directions for N = 2.

Using eqn (5) and (6), the transmission and density of states of the corresponding nanoribbons are calculated. As presented in Fig. 7, ZZ–b_{010}-Gallenene nanoribbon shows an interesting linear transmission related to the conduction band in Fig. 6(c) near the Fermi level. Notably, the zero transmission arises from the 0.35 (eV) band gap in its band structure. As shown in

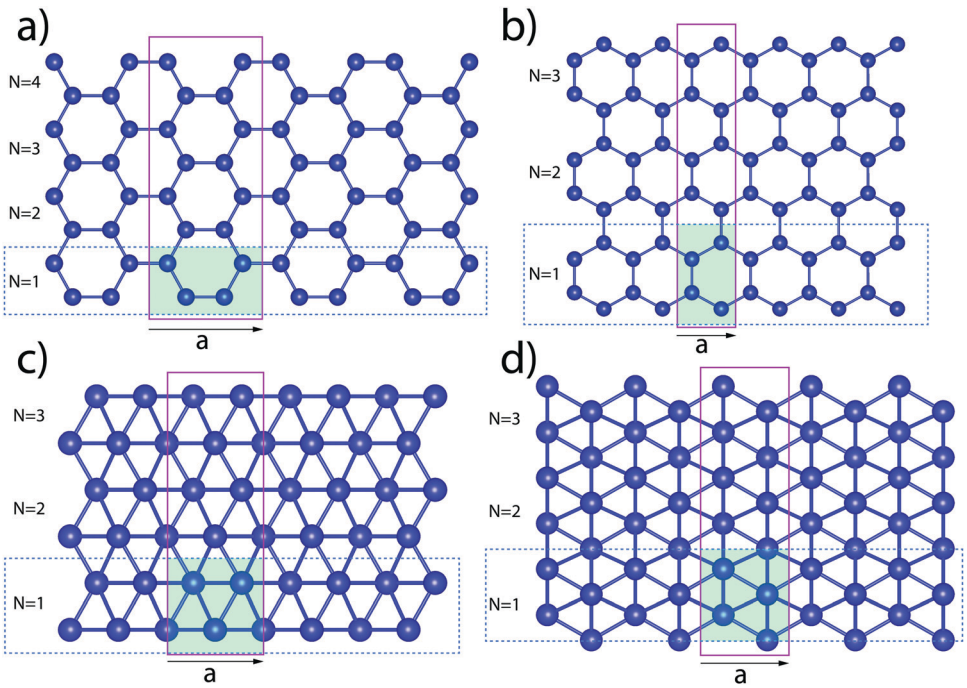

Fig. 5 The structure of a_{100}-Gallenene nanoribbon in the (a) x and (b) y direction and also b_{010}-Gallenene nanoribbon in the (c) x and (d) y direction. The unit cell is given by the solid line box. The dashed line represents the periodic chain labeled by N = 1, 2, 3,... which determines the width of the ribbon.

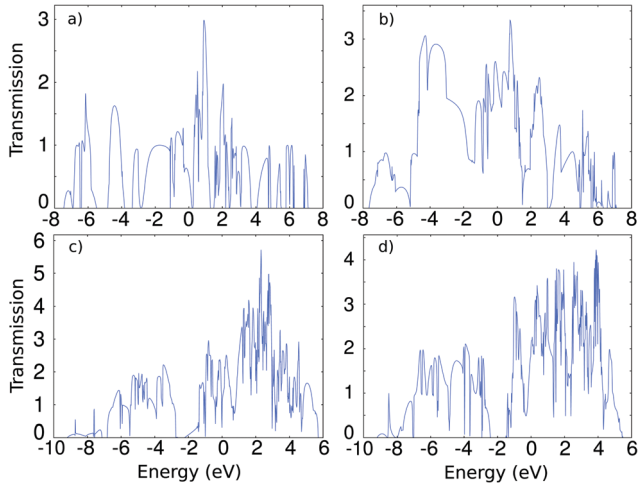

Fig. 7 Transmission of the nanoribbons of a_{100}-Gallenene in AC (a) and ZZ (b) directions and b_{010}-Gallenene in AC (c) and ZZ (d) directions for N = 2.

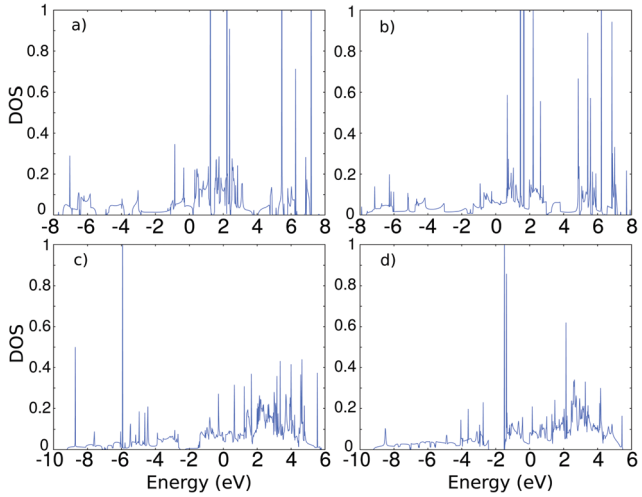

Fig. 8 Density of states for the ribbons of a_{100}-Gallenene in AC (a) and ZZ (b) directions and b_{010}-Gallenene in AC (c) and ZZ (d) directions for N = 2.

Fig. 6(d), ZZ–b_{010}-Gallenene nanoribbon has a 0.97 (eV) band gap which is much larger than that of the AC nanoribbon.

Moreover, the density of states for the nanoribbons are presented in Fig. 8. AC–a_{100}-Gallenene nanoribbon displays a linear density of states near the Fermi level which is evidence of a Dirac point in the Fermi level. As shown in Fig. 6(a), AC–a_{100}-Gallenene nanoribbon has a Dirac point around the X point in the BZ. The gaps for both nanoribbons of b_{010}-Gallenene are in agreement with the band-structure calculations shown in Fig. 6(c) and (d). It should be noted that the linear transmission related to the AC–b_{010}-Gallenene nanoribbon shows a constant density of states as presented in Fig. 8(c) near the Fermi level.

6 Summary

In summary, based on symmetry aspects and the LCAO method combined with first-principles calculations, we derived a TB model for two stabilized monolayer Gallenene structures. An orthogonal TB model was presented for a_{100}-Gallenene limited to the second nearest neighbors. b_{010}-Gallenene has a buckled structure with a high packing fraction which led us to construct a TB model based on a non-orthogonal basis set. In order to construct a TB model based on the simplified LCAO, we followed the SK approach in which the energy dispersion was fitted to the one obtained from DFT calculations. We determined the SK coefficients in a non-orthogonal basis set for monolayers of a_{100}-Gallenene and b_{010}-Gallenene which allows one to calculate different electronic properties using Green's function theory, *e.g.* electrical transport, tunneling, and the effect of impurities and defects on different electronic properties. The full expression for the Hamiltonian and overlap matrices for a_{100}-Gallenene and b_{010}-Gallenene are given in the ESI.† Moreover, the transmission properties of nanoribbons of both monolayers oriented along the AC and ZZ directions were also investigated and it was shown that both AC- and ZZ–b_{010}-Gallenene nanoribbons exhibit semiconducting behavior with zero transmission while a_{100}-Gallenene nanoribbons are metallic.

Conflicts of interest

There are no conflicts to declare.

Acknowledgements

This work is supported by the Methusalem program of the Flemish government and the FLAG-ERA project TRANS-2D-TMD. This work is supported by the Flemish Science Foundation (FWO-Vl) by a post-doctoral fellowship (M. Y.). M. N. is partially supported by BFO (Uantwerpen).

References

1 K. S. Novoselov, A. K. Geim, S. V. Morozov, D. Jiang, Y. Zhang, S. V. Dubonos, I. V. Grigorieva and A. A. Firsov, *Science*, 2004, **306**, 666.
2 A. K. Geim and K. S. Novoselov, *Nat. Mater.*, 2007, **6**, 183.
3 K. K. Kim, A. Hsu, X. Jia, S. M. Kim, Y. Shi, M. Hofmann, D. Nezich, J. F. Rodriguez-Nieva, M. Dresselhaus, T. Palacios and J. Kong, *Nano Lett.*, 2012, **12**, 161.
4 S. Manzeli, D. Ovchinnikov, D. Pasquier, O. V. Yazyev and A. Kis, *Nat. Rev. Mater.*, 2017, **2**, 17033.
5 J. N. Coleman, M. Lotya, A. O'Neill, S. D. Bergin, P. J. King, U. Khan, K. Young, A. Gaucher, S. De, R. J. Smith, I. V. Shvets, S. K. Arora, G. Stanton, H. Y. Kim, K. Lee, G. T. Kim, G. S. Duesberg, T. Hallam, J. J. Boland, J. J. Wang, J. F. Donegan, J. C. Grunlan, G. Moriarty, A. Shmeliov, R. J. Nicholls, J. M. Perkins, E. M. Grieveson, K. Theuwissen, D. W. McComb, P. D. Nellist and V. Nicolosi, *Science*, 2011, **331**, 568.
6 M. Chhowalla, H. S. Shin, G. Eda, L. J. Li, K. P. Loh and H. Zhang, *Nat. Chem.*, 2013, **5**, 263.

7 A. Kara, H. Enriquez, A. P. Seitsonen, L. C. L. Y. Voon, S. Vizzini, B. Aufray and H. Oughaddou, *Surf. Sci. Rep.*, 2012, **67**, 1.
8 P. Vogt, P. Padova, C. Quaresima, J. Avila, E. Frantzeskakis, M. C. Asensio, A. Resta, B. Ealet and G. L. Lay, *Phys. Rev. Lett.*, 2012, **108**, 155501.
9 P. D. Padova, O. Kubo, B. Olivieri, C. Quaresima, T. Nakayama, M. Aono and G. Le Lay, *Nano Lett.*, 2012, **12**, 5500.
10 E. Bianco, S. Butler, S. Jiang, O. D. Restrepo, W. Windl and J. E. Goldberger, *ACS Nano*, 2013, **7**, 4414.
11 M. Derivaz, D. Dentel, R. Stephan, M.-C. Hanf, A. Mehdaoui, P. Sonnet and C. Pirri, *Nano Lett.*, 2015, **15**, 2510.
12 M. E. Dávila, L. Xian, S. Cahangirov, A. Rubio and G. Le Lay, *New J. Phys.*, 2014, **16**, 095002.
13 M. E. Dávila and G. L. Lay, *Sci. Rep.*, 2016, **6**, 20714.
14 F.-f. Zhu, W.-j. Chen, Y. Xu, C.-l. Gao, D.-d. Guan, C.-h. Liu, D. Qian, S.-C. Zhang and J.-f. Jia, *Nat. Mater.*, 2015, **14**, 1020.
15 S. Saxena, R. P. Chaudhary and S. Shukla, *Sci. Rep.*, 2016, **6**, 31073.
16 L. Li, Y. Yu, G. J. Ye, Q. Ge, X. Ou, H. Wu, D. Feng, X. H. Chen and Y. Zhang, *Nat. Nanotechnol.*, 2014, **9**, 372.
17 H. Sachdev, *Science*, 2015, **350**, 1468.
18 Y. Xu, B. Yan, H.-J. Zhang, J. Wang, G. Xu, P. Tang, W. Duan and S.-C. Zhang, *Phys. Rev. Lett.*, 2013, **111**, 136804.
19 S.-C. Wu, G. Shan and B. Yan, *Phys. Rev. Lett.*, 2014, **113**, 256401.
20 A. Barfuss, L. Dudy, M. R. Scholz, H. Roth, P. Höpfner, C. Blumenstein, G. Landolt, J. H. Dil, N. C. Plumb, M. Radovic, A. Bostwick, E. Rotenberg, A. Fleszar, G. Bihlmayer, D. Wortmann, G. Li, W. Hanke, R. Claessen and J. Schäfer, *Phys. Rev. Lett.*, 2013, **111**, 157205.
21 Y. Ohtsubo, P. L. Fëvre, F. Bertran and A. Taleb-Ibrahimi, *Phys. Rev. Lett.*, 2013, **111**, 216401.
22 S. A. Yang, H. Pan and F. Zhang, *RSC Adv.*, 2015, **5**, 83350.
23 B. A. Bernevig and T. L. Hughes, *Topological Insulators and Topological Superconductors*, Princeton University Press, 2013.
24 F. D. M. Haldane, *Phys. Rev. Lett.*, 1988, **61**, 2015.
25 H. Zhang, C.-X. Liu, X.-L. Qi, X. Dai, Z. Fang and S.-C. Zhang, *Nat. Phys.*, 2009, **5**, 438.
26 Y. Xia, D. Qian, D. Hsieh, L. Wray, A. Pal, H. Lin, A. Bansil, D. Grauer, Y. S. Hor, R. J. Cava and M. Z. Hasan, *Nat. Phys.*, 2009, **5**, 398.
27 C. L. Kane and E. J. Mele, *Phys. Rev. Lett.*, 2005, **95**, 146802.
28 V. Derakhshan and S. A. Ketabi, *Physica E*, 2017, **85**, 253.
29 V. Kochat, A. Samanta, Y. Zhang, S. Bhowmick, P. Manimunda, S. Asif, A. S. Stender, R. Vajtai, A. K. Singh, C. S. Tiwary and P. M. Ajayan, *Sci. Adv.*, 2018, **4**, e1701373.
30 M. Bernasconi, G. L. Chiarotti and E. Tosatti, *Phys. Rev. B: Condens. Matter Mater. Phys.*, 1995, **52**, 9988.
31 T. Kenichi, K. Kazuaki and A. Masao, *Phys. Rev. B: Condens. Matter Mater. Phys.*, 1998, **58**, 2482.
32 L. Bosio, *J. Chem. Phys.*, 1978, **68**, 1221.
33 K. G. Steenbergen and N. Gaston, *Phys. Chem. Chem. Phys.*, 2013, **15**, 15325.
34 O. Schulte and W. Holzapfel, *Phys. Rev. B: Condens. Matter Mater. Phys.*, 1997, **55**, 8122.
35 M. Elstner, D. Porezag, G. Jungnickel, J. Elsner, M. Haugk, T. Frauenheim, S. Suhai and G. Seifert, *Phys. Rev. B: Condens. Matter Mater. Phys.*, 1998, **58**, 7260.
36 B. Aradi, B. Hourahine and T. Frauenheim, *J. Phys. Chem. A*, 2007, **111**, 5678.
37 J. C. Slater and G. F. Koster, *Phys. Rev.*, 1954, **94**, 1498.
38 D. A. Papaconstantopoulos and M. J. Mehl, *J. Phys.: Condens. Matter*, 2003, **15**, R413.
39 G. Kresse and J. Hafner, *Phys. Rev. B: Condens. Matter Mater. Phys.*, 1993, **47**, 558.
40 J. P. Perdew, K. Burke and M. Ernzerhof, *Phys. Rev. Lett.*, 1996, **77**, 3865.
41 K. Levenberg, *Q. Appl. Math.*, 1944, **2**, 164.
42 W. C. Lu, C. Z. Wang, K. Ruedenberg and K. M. Ho, *Phys. Rev. B: Condens. Matter Mater. Phys.*, 2005, **72**, 205123.
43 C. M. Goringe, D. R. Bowler and E. Hernandez, *Rep. Prog. Phys.*, 1997, **60**, 1447.
44 W. Kutzelnigg, *THEOCHEM*, 1988, **169**, 403.
45 S. D. Deshpande and R. B. Pode, *Am. J. Phys.*, 1988, **56**, 362.
46 E. A. Moore and L. E. Smart, *Solid state chemistry: an introduction*, CRC Press, 2012.
47 ESI†.
48 D. S. Fisher and P. A. Lee, *Phys. Rev. B: Condens. Matter Mater. Phys.*, 1981, **23**, 6851.
49 W. A. Harrison, *Electronic Structure and the Properties of Solids*, Dover Publications, 1989.
50 M. Kuno, *Introductory nanoscience: Physical and chemical concepts*, MRS Bulletin, 2012.
51 N. W. Ashcroft and N. D. Mermin, *Solid state physics*, Holt, Rinehart and Winston, New York, 1976.
52 S. Badalov, M. Yagmurcukardes, F. M. Peeters and H. Sahin, *J. Phys. Chem. C*, 2018, **122**, 28302.